ACS Photonics

pubs.acs.org/journal/apchd5

Article

Flexible Manipulation of Lasing Modes in an Erbium-Doped Microcavity via an Add−Drop Configuration

Song Zhu, Wenyu Wang, Bo Jiang, Linhao Ren, Lei Shi,* and Xinliang Zhang

Cite This: https://doi.org/10.1021/acsphotonics.1c01096

Read Online

ACCESS | Metrics & More | Article Recommendations | Supporting Information

ABSTRACT: Whispering-gallery-mode microlaser is an important candidate for various applications such as optical sensing, spectroscopy, and communications. The ability to manipulate lasing modes and even to realize single-mode lasing emission is highly desirable. Here, we realize flexible manipulation of lasing modes in an erbium-doped silica microbottle cavity via an add−drop configuration, which possesses highly nondegenerate modes along its axial direction. An ultralow lasing threshold down to 89 μW is achieved in the erbium-doped microbottle cavity with ultrahigh quality factors up to 10^8 via a novel doping method. We realize selective suppression and extraction of the lasing modes by coupling a probe microfiber at different axial positions of the microbottle cavity. Importantly, a single-mode microlaser with a high side-mode suppression ratio up to 24 dB is achieved without mode hopping. Our scheme demonstrated here may have various promising applications ranging from single-mode lasing emission and switchable microlaser to optical communication.

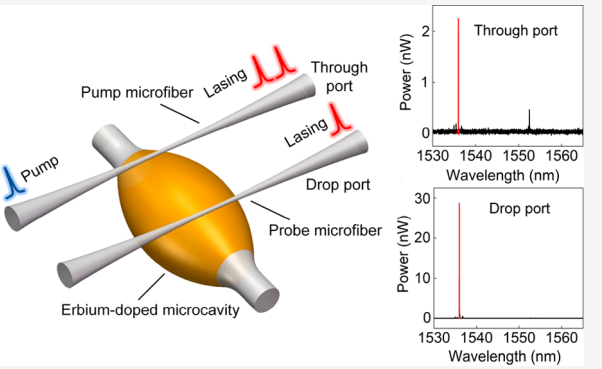

KEYWORDS: *whispering-gallery-mode microlaser, lasing-mode manipulation, single-mode lasing emission, erbium-doped microcavity, add−drop configuration*

Whispering-gallery-mode (WGM) microcavities are an excellent platform for realizing a low-threshold and narrow-linewidth laser due to its high quality (Q) factor (i.e., low loss) and small footprint (i.e., small mode volume (V_m)).[1−4] Up to now, there are many kinds of gain materials used for WGM lasing emission, such as dyes,[5] semiconductors,[6−11] conjugated polymers,[12] gold nanorods,[13] and rare earth elements.[14−19] Rare earth elements have captured much interest because of the large quantum efficiency and ease of emitting in the infrared wavelength band.[20]

Lasing mode manipulation is highly desirable, such as single-mode lasing emission,[21,22] suppression of lasing modes,[23] selectivity of lasing wavelength,[24,25] and controllable vortex lasing generation.[26] Meanwhile, selective emission of lasing modes, especially single-mode lasing emission, is of importance for optical communications. Up to now, there are several proposed schemes, which realized mode manipulation of WGM lasing and even single-mode lasing emission, such as spatial pump engineering,[21,22] loss engineering,[23] parity-time symmetric coupled cavities,[27] and cavity size engineering.[28] However, these proposed methods have disadvantages, such as sacrificed Q factors induced by the decreased cavity size or lack of flexibility. The ultrahigh-Q silica microcavity is a good candidate to achieve an ultralow-threshold and ultranarrow-linewidth laser.[29−32] Silica microbottle cavities have been given much attention and applied in various areas, such as cavity quantum electrodynamics, cavity optomechanics, microlaser, and so on.[16,33,34] There are rich WGMs and, thus, lasing modes that can be selectively excited in the microbottle cavity due to its parabolic profile. Since it has nondegenerate axial symmetrical modes, this makes optical gain shared by multiple lasing modes, which leads to optical instability due to mode competition.[35] However, it is difficult to reduce the number of lasing modes and even realize a single-mode laser through a single coupling microfiber for the microbottle laser.

Here, we propose and demonstrate flexible manipulation of the lasing modes in the erbium-doped silica microbottle cavity through an add−drop configuration. A novel erbium doping method is demonstrated, which leads to a lasing threshold as low as 89 μW, pumped by a 974 nm diode laser. As shown in Figure 1a, an optical microfiber is used to couple pump light into the microbottle cavity while outputting the laser through this port. Another microfiber acts as a probe, which can reduce the number of lasing modes and also selectively extract specific lasing modes. Based on the add−drop configuration, we first realize selective extraction of the lasing modes in the

Received: July 19, 2021

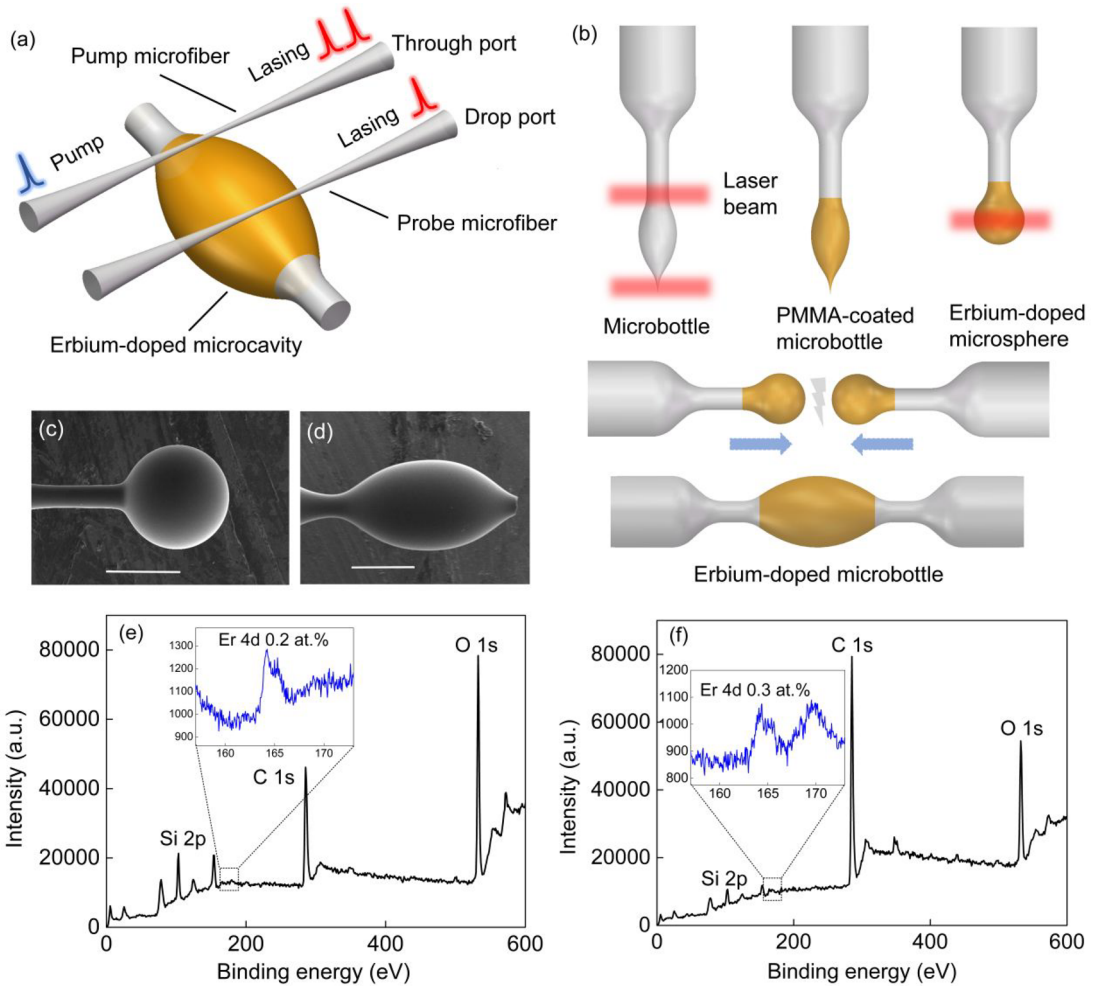

Figure 1. (a) Illustration of flexible manipulation of lasing modes in an erbium-doped silica microbottle cavity. (b) Fabrication process of an erbium-doped silica microbottle cavity. Scanning electron microscope (SEM) images of (c-d) the erbium-doped microsphere (scale bar: 50 μm) and microbottle (scale bar: 50 μm) cavities, respectively. XPS spectra of the erbium-doped microcavities after etched by (e) ~1 and (f) ~3 μm.

microlaser and even single-mode lasing emission with a side-mode suppression ratio as high as 24 dB.

DEVICE FABRICATION

In this work, two silica microfibers with losses smaller than 0.3 dB are fabricated through the flame-heated technique.[36] Erbium-doped silica microcavities can be fabricated through the ion implantation method[37] and the sol−gel method[14] with a complex process or relatively low Q factors. Therefore, we proposed an erbium doping method that can achieve ultrahigh Q factors of the doped microcavity,[16] but most of the erbium ions are only located on the surface of the microcavity, which minimizes the field overlap between the erbium ions and the WGMs. Here, we propose a novel doping method, which enables erbium ions to be doped into the interior of a microcavity and results in a large field overlap between the erbium ions and the WGMs. The fabrication process is illustrated in Figure 1b. A single-mode fiber is first vertically fixed on a carbon dioxide (CO_2) laser fabrication platform and then is tapered into a bottle profile by two laser beams. After that, the bottle area is dipped into the erbium-dissolved poly(methyl methacrylate) (PMMA) solution for ~10 s and then is taken out. (For the synthesis of the PMMA solution, erbium solution, and erbium-dissolved PMMA solution, see part S1 in the Supporting Information.) After acetone is evaporated from the PMMA solution, the PMMA-coated microbottle is fused into a microsphere by the two laser beams. Coated PMMA is burnt out and erbium ions are naturally doped into the microsphere. Finally, two doped microspheres are mounted on the commercial fused splicer and then an erbium-doped microbottle cavity is fabricated by arc discharge. The novel doping method can enable erbium ions to be uniformly doped into the silica microbottle cavity. Figure 1c shows a scanning electron microscope (SEM) image of the erbium-doped microsphere cavity with a diameter of 70 μm. Figure 1d is a SEM image of the erbium-doped microbottle cavity with an equatorial diameter of 74 μm fabricated from two microspheres. The method can effectively increase the overlap between the erbium ions and the WGMs while maintaining the ultrahigh Q factor of the doped microcavity compared with the method in our previous work.[16] In order to verify this point, we measure the X-ray photoelectron spectroscopy (XPS) of the erbium-doped microbottle cavity, as shown in Figure 1e,f. As shown in Figure S1 in the Supporting Information, the fundamental mode and the second-order mode are located at 1 and 2.7 μm away from the bottle surface, respectively. (For WGM simulations, see part S2 in the Supporting Information.) In order to measure the existence of the erbium element in the WGM areas, the erbium-doped microcavities (volume ratio = 1:20) are etched

https://doi.org/10.1021/acsphotonics.1c01096
ACS Photonics XXXX, XXX, XXX−XXX

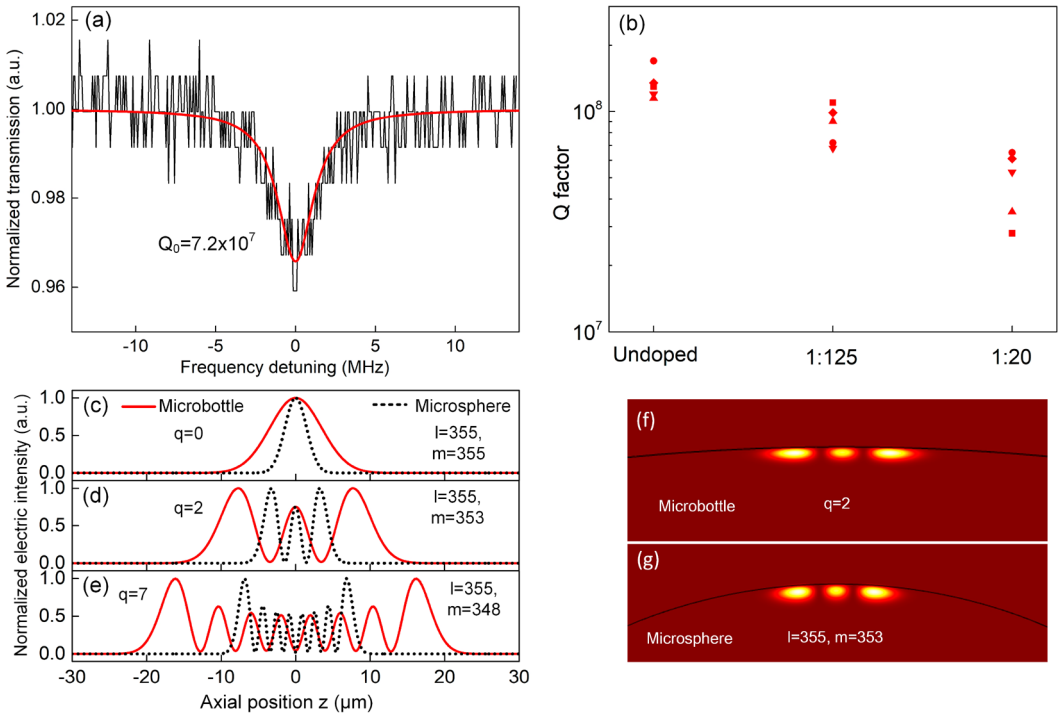

Figure 2. (a) Typical transmission spectrum of an erbium-doped microbottle cavity. (b) Intrinsic Q factors of a series of undoped and doped microcavities (volume ratios = 1:125 and 1:20). (c−e) Field distributions with different axial orders in a microbottle cavity and with different angular orders in a microsphere cavity. q is the axial order of WGMs in the microbottle cavity. l and m are the angular and azimuthal orders of WGMs in the microsphere cavity, respectively. (f, g) Two-dimensional (2D) field distributions of the microbottle and microsphere cavities.

for ∼1 and ∼3 μm by hydrofluoric acid (HF), respectively. As shown in Figure 1e, the high-resolution XPS spectrum shows the existence of the erbium element at 1 μm away from the bottle surface, with a binding energy peak of ∼165 eV. Figure 1f shows the existence of the erbium element at 3 μm away from the bottle surface. It is worth noting that the percentage of the erbium element at 1 μm (0.2 at. %) is close to that at 3 μm (0.3 at. %), which means that the erbium ions are uniformly doped into the microcavity and have a large overlap with the WGMs.

RESULTS AND DISCUSSION

Figure 2a shows the transmission spectrum of a specific mode in the doped microbottle cavity, which is fabricated from the erbium-dissolved PMMA solution with a volume ratio of 1:125 and a high loaded Q factor of 7×10^7 at 1550 nm is realized, which corresponds to an intrinsic Q factor (Q_0) of 7.2×10^7. We also measure Q factors of a set of doped and undoped cavities with equatorial diameters of ∼125 μm, as shown in Figure 2b. It can be seen that the intrinsic Q factors of the undoped cavities are above 10^8, which illustrates a fact that this fabrication method can result in ultralow scattering losses and ultrahigh Q factors. After being doped with erbium ions (volume ratio = 1:125), the intrinsic Q factors decrease a little, which are still above 10^7 and even exceeding 10^8, and decrease with each increment of the ion concentration (volume ratio = 1:20) due to the increased absorption loss.[38] (For analysis of the Q factor for the microcavity with an add−drop structure, see part S3 in the Supporting Information.) In addition, we fabricated another 15 devices to measure their Q factors and corresponding lasing thresholds. The results show that the fabrication method also has a good reproducibility. (For details, see part S4 in the Supporting Information.)

The microbottle cavity has a smaller curvature compared with the microsphere cavity,[39] thus, the axial modes are well separated by large spacings along the axial direction. As shown in Figure 2c−e, the mode distributions with different axial orders (q) in the microbottle cavity and with different azimuthal orders ($m = -l, -l + 1, ..., l - 1, l$) in the microsphere cavity are calculated, respectively.[16,40] It can be found that the axial modes in the microbottle cavity are less compact than the azimuthal modes in the microsphere cavity. It enables us to easily extract a specific lasing mode by a probe microfiber at different coupling positions along the axial direction of the microbottle cavity. Both the microbottle and the microsphere cavities used for calculations have diameters of 126 μm. Figure 2f,g demonstrates 2D mode distributions of the microbottle and microsphere cavities, respectively, which correspond to the modes shown in Figure 2d.

The proposed doping method is also suitable for fabricating the erbium-doped microbottle cavities with the smaller equatorial diameter, thus we fabricate the microbottle cavities with equatorial diameters of 82, 101, 137, and 187 μm. Figure 3a−d shows optical microscope images of the doped microbottle cavities with different equatorial diameters. All of them are attached on the fiber stems. The lasing thresholds of the doped microbottle cavities are also measured. In order to avoid instability of the coupling between the microfiber and the microcavity, both of the two microfibers are in touch with the microcavity in the experiments. Figure 3e shows the output lasing power as a function of the pump power for different equatorial diameters. Consequently, it can be seen that the thresholds are around 100 μW and the minimum threshold down to 89 μW is realized, which is lower than those realized through nonresonant pump in previous works.[16,17,41,42] It means a fact that erbium ions can be effectively and easily

https://doi.org/10.1021/acsphotonics.1c01096
ACS Photonics XXXX, XXX, XXX−XXX

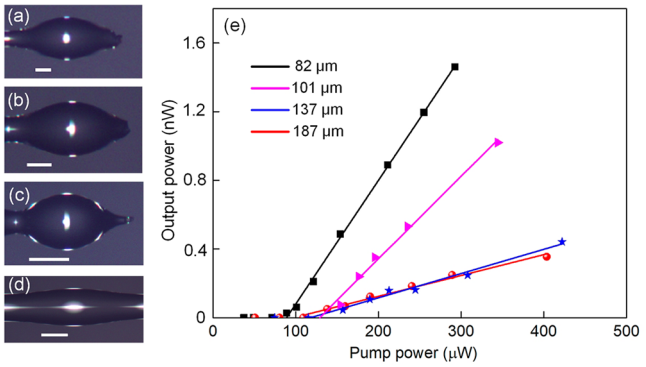

Figure 3. (a–d) Optical microscopes images of the microbottle cavities with equatorial diameters of 82 μm (scale bar: 30 μm), 101 μm (scale bar: 50 μm), 137 μm (scale bar: 100 μm), and 187 μm (scale bar: 125 μm), respectively. (e) Output lasing power as a function of the pump power for the microbottle cavities with different equatorial diameters.

doped into the silica microbottle cavities regardless of their sizes. A microfiber is used to couple 974 nm laser with a linewidth of ~1 nm into the microcavity. Here, for the microbottle cavity with a diameter of 126 μm and a curvature (Δk) of 0.0073 μm^{-1}, its axial free spectral range (FSR) is calculated as 2 nm according to the equation: $\Delta\lambda_q = \Delta k\lambda^2/2\pi n_{eff}$.[36] Due to the nondegenerate WGMs in the microbottle cavity, the linewidth of the pump laser can cover a number of WGMs, which corresponds to nonresonant pump compared with resonant pump.[14,43,44]

The inset in Figure 4d shows an optical microscope image of a doped microbottle cavity with an equatorial diameter of 126 μm and a bottle length of 248 μm. The outer profile of the microbottle can be fitted by parabola, which is expressed by $R(z) = R(0)[1 - (\Delta k z)^2/2]$,[36] where $R(z)$ represents the outer radius as a function of the axial position (z), Δk denotes the bottle curvature. Here, $R(0) = 63$ μm, $z_{max} = 124$ μm, and $\Delta k = 0.0073$ μm^{-1}. There are symmetrical axial mode distributions in the microbottle cavity, thus, we measure the lasing spectra by putting the pump microfiber at different positions along the axial direction of the microbottle cavity. Figure 4a–c demonstrates the output lasing spectra when it is pumped at 0, 30, and 63 μm away from the bottle center, respectively. It can be seen that the lasing modes with different orders can be easily switched by adjusting the pump position.[45] Besides, as shown in Figure 4d, it is worth noting that the minimum lasing threshold of 154 μW is achieved and increases with increment of the pump position away from the bottle center. The maximum lasing threshold of 414 μW is achieved when the microfiber is at 63 μm away from the bottle center. It is because the Purcell factor is inversely proportional to V_m according to the equation: $F = \frac{3Q}{4\pi^2 V_m}\cdot\left(\frac{\lambda_m}{n}\right)^3$, where λ_m is the resonant wavelength, n is the refractive index (RI) of silica, which leads to the higher lasing threshold.[46] (For V_m calculations of WGMs in the microbottle cavity, see part S5 in the Supporting Information.)

Microcavity-based add-drop configuration is a functional structure, which is an excellent candidate for multiports resonant filters,[47] optical switching,[48] and second harmonic generation (SHG).[49] Generally, most of add-drop structures are in the equators of the cavities due to the geometric limitation.[47] For an add-drop structure based on the microbottle cavity, there are highly nondegenerate WGMs with different orders along its axial direction,[50] thus, it is possible to selectively extract desired modes by adjusting the coupling position of the probe microfiber. For the erbium-doped microbottle cavity, it is possible to selectively extract specific lasing modes using an add–drop structure. Two microfibers with diameters of 1.26 and 2.2 μm act as a pump microfiber and a probe microfiber, respectively. As shown in the inset of Figure 5a, the pump microfiber is put at 63 μm away from the bottle center, thus, the pump light can be coupled into the microcavity and excite the high-order modes

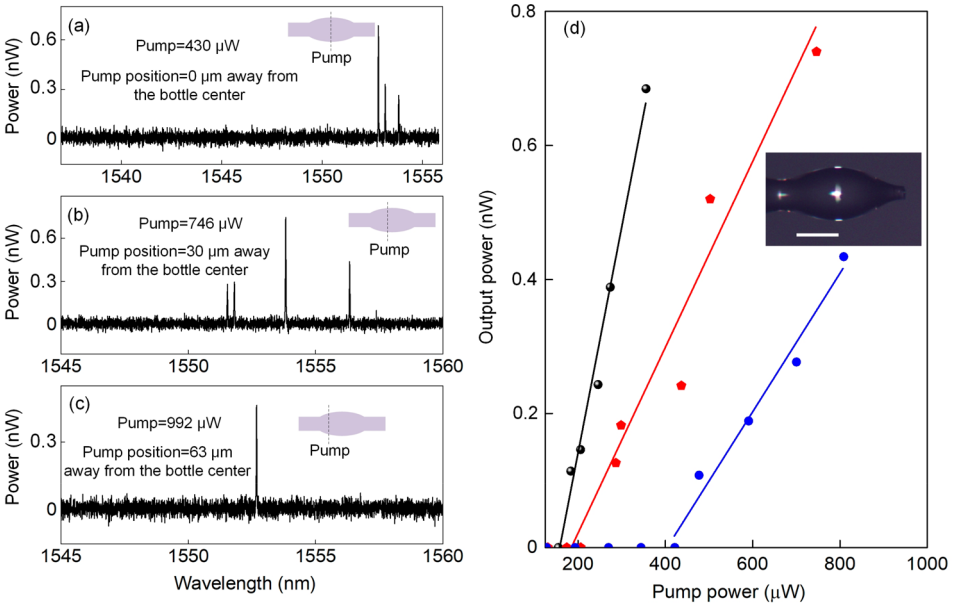

Figure 4. (a–c) Output lasing spectra pumped at different positions of the microbottle cavity. Insets in (a)–(c) illustrate the coupling positions of the pump microfiber (dashed black line) along the axial direction of the microbottle cavity. (d) Output lasing power as a function of the pump power. The inset is an optical microscope image of the doped microbottle cavity with an equatorial diameter of 126 μm. Scale bar: 100 μm.

https://doi.org/10.1021/acsphotonics.1c01096
ACS Photonics XXXX, XXX, XXX–XXX

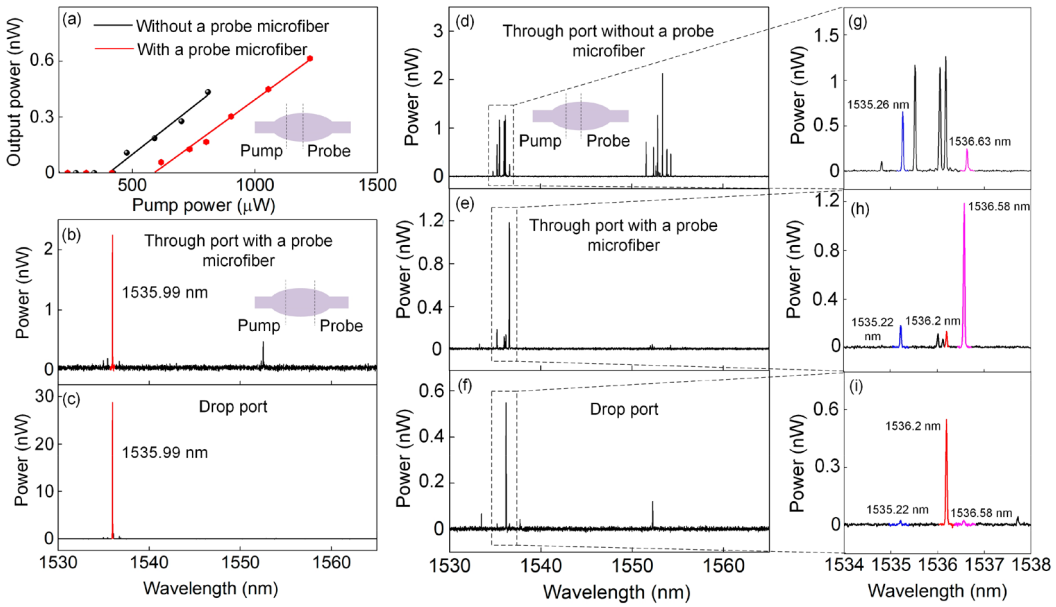

Figure 5. (a) Output lasing power as a function of the pump power without and with a probe microfiber (at the bottle center). Lasing spectra from (b) a through port (at 63 μm away from the bottle center) with a probe microfiber and (c) a drop port (at 63 μm away from the bottle center). Lasing spectra from (d) a through port (at 63 μm away from the bottle center) without a probe microfiber, (e) a through port with a probe microfiber (at the bottle center), and (f) a drop port. (g) Zoom-in spectrum of (d). (h) Zoom-in spectrum of (e). (i) Zoom-in spectrum of (f).

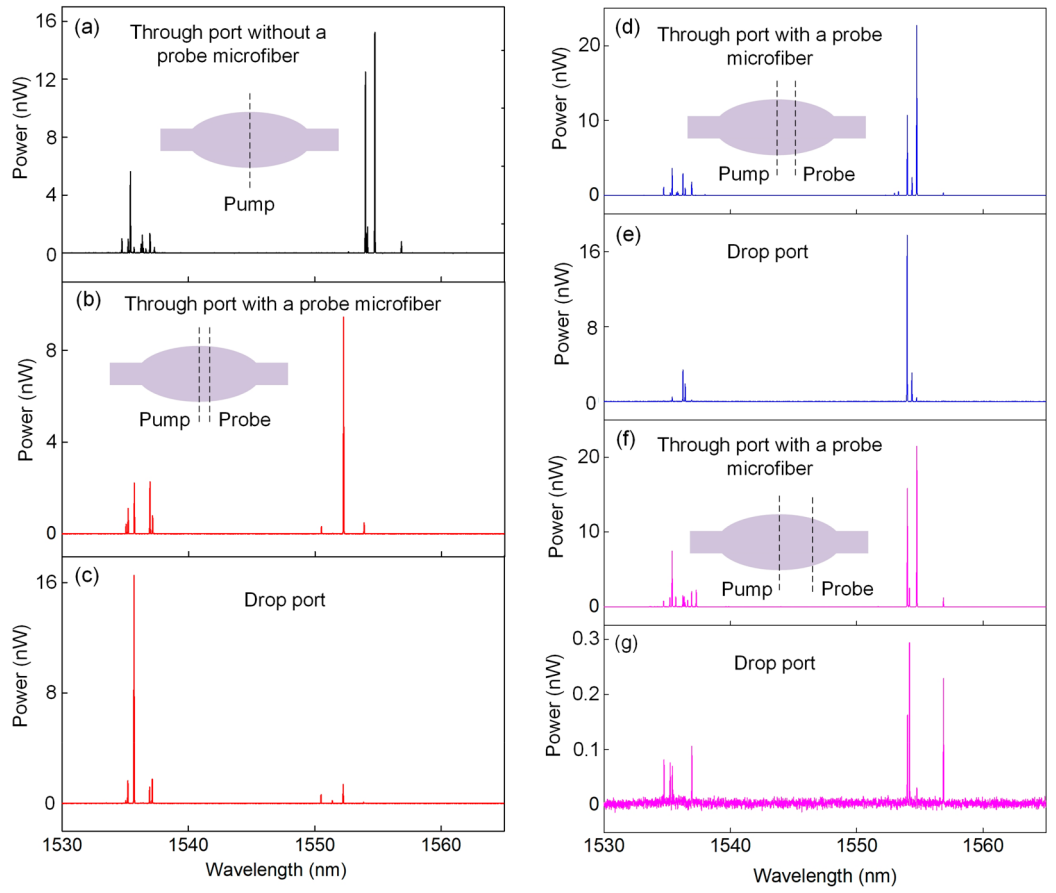

Figure 6. (a) Output lasing spectrum of the microbottle cavity pumped at the bottle center without a probe microfiber. Output lasing spectra from (b) a through port (at the bottle center) with a probe microfiber (at 30 μm away from the bottle center) and (c) a drop port. Output lasing spectra from (d) a through port with a probe microfiber (at 46 μm away from the bottle center) and (e) a drop port. Output lasing spectra from (f) a through port with a probe microfiber (at 75 μm away from the bottle center) and (g) a drop port.

https://doi.org/10.1021/acsphotonics.1c01096
ACS Photonics XXXX, XXX, XXX−XXX

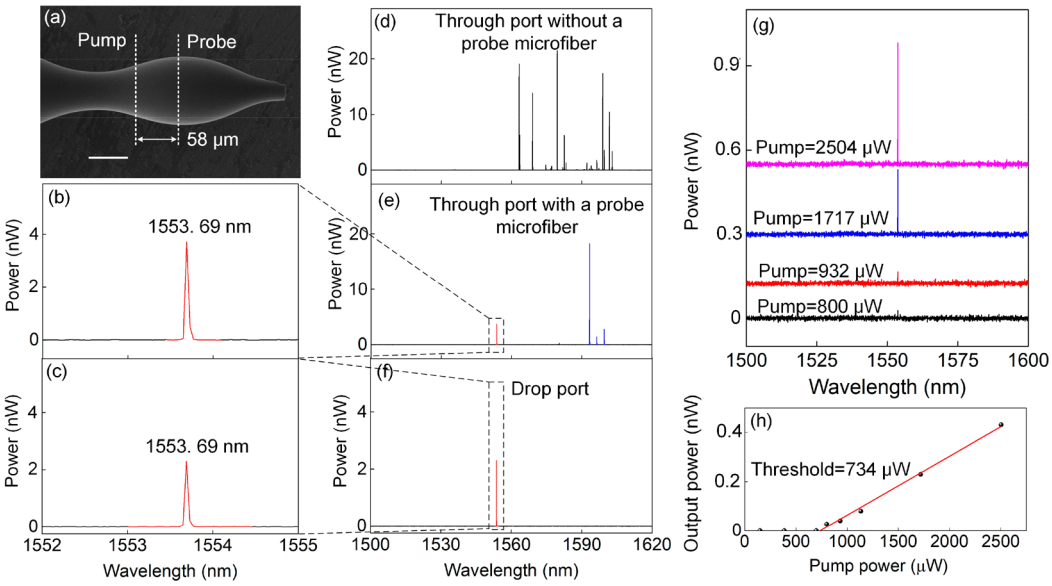

Figure 7. (a) SEM image of the microbottle cavity with an equatorial diameter of 88 μm. Dashed lines represent the coupling positions of the pump microfiber and the probe microfiber, respectively. Scale bar: 50 μm. (b) Enlarged lasing spectrum of (e). (c) Enlarged lasing spectrum of (f). (d) Lasing spectrum of the microbottle cavity pumped at 58 μm away from the bottle center. (e) Lasing spectrum of the through port (at 58 μm away from the bottle center) with a probe microfiber (at the bottle center). (f) Lasing spectrum from the drop port. The pump power is 7.165 mW. (g) Evolution of a single-mode laser with increment of the pump power. (h) Output lasing power of the single-mode laser from the drop port as a function of the pump power.

at the 974 nm band, which can effectively pump most erbium ions in the microbottle cavity since the high-order modes spatially distribute in a large area along its axial direction.[36] In order to suppress the number of lasing modes and selectively extract lasing modes, the probe microfiber is put in the center of the microbottle cavity. The reason why the probe microfiber is thicker than the pump microfiber is that the effective refractive indexes (n_{eff}) of the lower-order WGMs are larger than those of the higher-order WGMs, thus, we can effectively extract the lower-order lasing modes located close to the bottle center. (For theoretical analysis of phase-matching condition, see part S6 in the Supporting Information.) We first measure the output lasing power as a function of the pump power, as shown in Figure 5a. The black line represents the output lasing power versus the pump power when there is no probe microfiber. The lasing threshold of 414 μW is achieved. After the probe microfiber is put at the center of the microbottle cavity, the lasing threshold increases to 600 μW. It is because the probe microfiber introduces extra coupling and scattering losses to the WGMs, which greatly improve the lasing threshold.[23,47] Figure 5d shows the lasing spectrum output from the through port with a pump power of 6.09 mW when there is no probe microfiber. The two lasing bands is derived from the two gain peaks in the gain spectrum of erbium element.[16] As shown in Figure 5e, when a probe microfiber is put at the bottle center, most of the lasing modes disappear in the spectrum output from the through port due to the increased loss. As shown in the lasing spectrum from the drop port in Figure 5f, there are only several lasing modes with an apparent lasing peak at 1536 nm. Figure 5g–i shows the enlarged lasing spectra of Figure 5d–f. As shown from the blue line in Figure 5g, the lasing peak is located at 1535.26 nm. The lasing peak for the same-order mode in Figure 5h is located at 1535.22 nm, which shows a 0.04 nm blue-shift compared with that in Figure 5g. The pink lines also show the same phenomenon. The blue-shift is because the probe microfiber leads to a decrease in the Q factors, which results in the decrease of the pump-induced energy accumulation in the microcavity, leading to a reduction in the thermal effect. By comparing the pink lines in Figure 5h and i, it can be seen that both of them have the same lasing wavelength, but the lasing power in Figure 5i is smaller than that in Figure 5h. It is because the extracting efficiency of the probe microfiber is lower than that of the pump microfiber. For the red line in Figure 5h, there is no corresponding lasing peak at 1536.2 nm, as shown in Figure 5g. It is because when the loss is introduced to certain lasing modes, these lasing modes will disappear and the others will emerge and dominate due to the reduction of mode competition. As shown in Figure 5i, the lasing peak power at 1536.2 nm is larger than that in Figure 5h. It may be because the extraction efficiency of the probe microfiber is higher for this mode. After that, the probe microfiber is moved to 63 μm away from the bottle center, which is symmetrical to the pump microfiber. From Figure 5b it can be seen that there are only four apparent lasing peaks in the lasing spectrum. The large decrease in the lasing-mode number is because the probe microfiber is located at the position, where it introduces the largest loss to the main lasing modes. From the lasing spectrum of the probe microfiber in Figure 5c, it is worth noting that there are only two apparent lasing peaks including one higher peak and one lower peak. The higher peak in the drop spectrum is consistent with that in the through spectrum in Figure 5b, which means a fact that this lasing mode is located at the position close to the microfiber coupling position. Besides, the laser spectrum from the drop port has a high side-mode suppression ratio of ~15 dB. It is worthy to note that the lasing modes can be selectively extracted by moving the probe microfiber to the different positions along the axial direction of the microbottle cavity.

As shown in Figure 6a, the pump microfiber is put at the bottle center with a pump power of 6.26 mW. In order to selectively extract lasing modes, the probe microfiber is

https://doi.org/10.1021/acsphotonics.1c01096
ACS Photonics XXXX, XXX, XXX−XXX

successively put at 30, 46, and 75 μm away from the bottle center, as shown in Figure 6b–g. Figure 6b shows the lasing spectrum from the through port after a probe microfiber is put at 30 μm away from the bottle center. Most of the lasing modes are apparently suppressed. From the lasing spectrum from the through port in Figure 6c it can be found that there is a high lasing peak at 1535.7 nm together with several weaker lasing peaks. Figure 6e,g is lasing spectra of the drop port when it is put at 46 and 75 μm away from the bottle center. It is worth noting that the lasing wavelengths are different among Figure 6c, e, and g. The wavelength differences are because the probe microfiber can effectively extract the specific lasing modes, which have the largest field overlap with the probe microfiber.[51] Therefore, the drop port can flexibly and selectively extract the lasing modes by moving its position along the axial direction of the microbottle cavity.

From Figure 5f it can be predicted that a single-mode lasing operation can be realized by putting the probe microfiber at an appropriate position. In order to decrease the number of lasing modes in the microcavity, it is necessary to decrease its diameter, which will effectively increase the resonant frequency difference among WGMs with different orders.[21,28] Besides, the microbottle cavity has the axial FSR, thus, it is also necessary to increase its axial FSR by increasing the bottle curvature (Δk). (For calculations of FSR vs the equatorial diameter and Δk, see part S7 in the Supporting Information.) Therefore, we fabricate an erbium-doped microbottle cavity with a smaller equatorial diameter (88 μm) and a larger Δk (0.0117 μm^{-1}), whose SEM image is shown in Figure 7a. Figure 7d shows the lasing spectrum from the through port with a pump power of 7.165 mW when there is no probe microfiber. There are still many apparent lasing peaks in the lasing spectrum, even though the equatorial diameter is decreased. Figure 7e shows the lasing spectrum from the through port after the probe microfiber is put at the bottle center and one lasing peak emerges around 1550 nm. From Figure 7f, it is worthy to note that the single-mode laser is extracted because this lasing mode has the maximum extracting efficiency by the probe microfiber. A high side-mode suppression ratio of ~24 dB is realized, which is much larger than that realized in the similar cavity structures.[21,23,52,53] By comparing Figure 7b and c, it can be seen that lasing from the two ports have the same center wavelength of 1553.69 nm. We also measure the evolution of the singe-mode laser with the increase of the pump power, as shown in Figure 7g. Importantly, it can be seen that there is no other lasing peak in this process, so mode hopping is effectively avoided. The lasing power from the drop port versus the pump power is shown in Figure 7h, it can be seen that a single-mode microlaser with a low threshold of 734 μW is realized. The proposed add–drop configuration is a flexible structure to achieve the ultralow-threshold single-mode lasing from the microbottle cavity.

CONCLUSION

In summary, we have demonstrated selective suppression and extraction of specific lasing modes, and even single-mode lasing emission in the erbium-doped microbottle cavities. Featuring the ultrahigh Q factor (exceeding 10^8) of the doped microcavity and the larger field overlap between the gain materials and the WGMs with the proposed erbium doping method, an ultralow lasing threshold of 89 μW is achieved by nonresonant pump, which is lower than most of the previous results through the same pump scheme. By taking an advantage of spatially well-separated distribution of the axial modes in the microbottle cavity, the number of lasing modes is decreased and the specific lasing modes are selectively extracted through an add–drop structure. Finally, single-mode lasing emission with a high side-mode suppression ratio of ~24 dB is realized without mode hopping. We believe that the proposed scheme will pave the way for a variety of applications including single-mode microlaser, laser switching and optical communication.

MATERIALS AND METHODS

Material Information. $Er(NO_3)_3{\cdot}5H_2O$ (99.9% meta basis) was purchased from Macklin. PMMA powder $[(C_5H_8O_2)]_n$ was bought from Tokyo Chemical Industry Co., Ltd.

Finite Element Method (FEM) Simulation. FEM simulations are used to calculate WGM distributions of the microbottle and microsphere cavities. The axial modes with different orders in the microbottle cavity and the modes with different azimuthal orders in the microsphere cavity were calculated by building up 2D axially symmetric models.

Experimental Test Setup. Experimental setup is illustrated in Figure S6 in part S8 in the Supporting Information. Signal light derived from a narrow-linewidth external-cavity laser working in the 1550 nm band is controlled by a polarization controller (PC). After that, it is coupled into the microbottle cavity to excite WGMs. The transmission spectrum is detected by a photodetector (PD) and is analyzed by a digital storage oscilloscope (DSO). Pump light coming from a 974 nm diode laser with a linewidth of ~1 nm is fed into a 20/80 optical splitter, and then is coupled into the erbium-doped microbottle cavity and a power meter (PM) is used to detect the pump power. The lasing spectra from the through port and the drop port are measured by an optical spectrum analyzer (OSA).

ASSOCIATED CONTENT

Supporting Information

The Supporting Information is available free of charge at https://pubs.acs.org/doi/10.1021/acsphotonics.1c01096.

Synthesis of the PMMA solution, erbium solution, and erbium-dissolved PMMA solution. WGM simulations. Q factor analysis. Reproducibility of the fabrication method. Mode volume (V_m) calculations. Analysis of coupling between the microfiber and the microcavity. Azimuthal FSR vs the equatorial diameter and axial FSR vs the bottle curvature. Experimental test setup (PDF)

AUTHOR INFORMATION

Corresponding Author

Lei Shi – *Wuhan National Laboratory for Optoelectronics, Huazhong University of Science and Technology, Wuhan 430074, China;* orcid.org/0000-0002-9961-6723; Email: lshi@hust.edu.cn

Authors

Song Zhu – *Wuhan National Laboratory for Optoelectronics, Huazhong University of Science and Technology, Wuhan 430074, China; School of Electrical and Electronic Engineering, Nanyang Technological University, Singapore 639798, Singapore*

https://doi.org/10.1021/acsphotonics.1c01096
ACS Photonics XXXX, XXX, XXX–XXX

Wenyu Wang − *Wuhan National Laboratory for Optoelectronics, Huazhong University of Science and Technology, Wuhan 430074, China*
Bo Jiang − *Wuhan National Laboratory for Optoelectronics, Huazhong University of Science and Technology, Wuhan 430074, China*
Linhao Ren − *Wuhan National Laboratory for Optoelectronics, Huazhong University of Science and Technology, Wuhan 430074, China*
Xinliang Zhang − *Wuhan National Laboratory for Optoelectronics, Huazhong University of Science and Technology, Wuhan 430074, China*

Complete contact information is available at: https://pubs.acs.org/10.1021/acsphotonics.1c01096

Author Contributions

S.Z. and L.S. conceived the idea. S.Z. and W.Y.W. designed and carried out the experiments and performed the data analysis. L.S. and X.L.Z. supervised the project. All authors discussed the results and reviewed the manuscript.

Notes

The authors declare no competing financial interest.

■ ACKNOWLEDGMENTS

This work was supported by the National Natural Science Foundation of China (11774110, 91850115), the Fundamental Research Funds for the Central Universities (HUST: 2019kfyXKJC036, 2019kfyRCPY092), the State Key Laboratory of Advanced Optical Communication Systems and Networks (2021GZKF003), and the State Key Laboratory of Applied Optics (SKLAO2021001A10).

■ REFERENCES

(1) Spillane, S.; Kippenberg, T.; Vahala, K. J. Ultralow-threshold Raman laser using a spherical dielectric microcavity. *Nature* **2002**, *415*, 621−623.
(2) Zhang, Z.; Qiao, X.; Midya, B.; Liu, K.; Sun, J.; Wu, T.; Liu, W.; Agarwal, R.; Jornet, J. M.; Longhi, S.; Litchinitser, N. M.; Feng, L. Tunable topological charge vortex microlaser. *Science* **2020**, *368*, 760−763.
(3) Toropov, N.; Cabello, G.; Serrano, M. P.; Gutha, R. R.; Rafti, M.; Vollmer, F. Review of biosensing with whispering-gallery mode lasers. *Light: Sci. Appl.* **2021**, *10*, 1−19.
(4) Fan, X.; Yun, S. H. The potential of optofluidic biolasers. *Nat. Methods* **2014**, *11*, 141−147.
(5) Gong, C.; Qiao, Z.; Yuan, Z.; Huang, S.; Wang, W.; Wu, P.; Chen, Y. Topological encoded vector beams for monitoring amyloid-lipid interactions in microcavity. *Adv. Sci.* **2021**, *8*, 2100096.
(6) Sun, Y.; Song, F.; Qian, C.; Peng, K.; Sun, S.; Zhao, Y.; Bai, Z.; Tang, J.; Wu, S.; Ali, H.; Bo, F.; Zhong, H.; Jin, K.; Xu, X. High-Q microcavity enhanced optical properties of $CuInS_2$/ZnS Colloidal quantum dots toward non-photodegradation. *ACS Photonics* **2017**, *4*, 369−377.
(7) Jana, S.; Xu, X.; Klymchenko, A.; Reisch, A.; Pons, T. Microcavity-enhanced fluorescence energy transfer from quantum dot excited whispering gallery modes to acceptor dye nanoparticles. *ACS Nano* **2021**, *15*, 1445−1453.
(8) Wang, Y.; Ta, V. D.; Leck, K. S.; Tan, B. H. I.; Wang, Z.; He, T.; Ohl, C. D.; Demir, H. V.; Sun, H. Robust whispering-gallery-mode microbubble lasers from colloidal quantum dots. *Nano Lett.* **2017**, *17*, 2640−2646.
(9) Tang, B.; Dong, H.; Sun, L.; Zheng, W.; Wang, Q.; Sun, F.; Jiang, X.; Pan, A.; Zhang, L. Single-mode lasers based on cesium lead halide perovskite submicron spheres. *ACS Nano* **2017**, *11*, 10681−10688.
(10) Zhang, Q.; Shang, Q.; Su, R.; Do, T. T. H.; Xiong, Q. Halide perovskite semiconductor lasers: materials, cavity design, and low threshold. *Nano Lett.* **2021**, *21*, 1903−1914.
(11) Wang, K.; Li, G.; Wang, S.; Liu, S.; Sun, W.; Huang, C.; Wang, Y.; Song, Q.; Xiao, S. Dark-field sensors based on organometallic halide perovskite microlasers. *Adv. Mater.* **2018**, *30*, 1801481.
(12) Tang, S.; Liu, Z.; Qian, Y.; Shi, K.; Sun, Y.; Wu, C.; Gong, Q.; Xiao, Y. A tunable optofluidic microlaser in a photostable conjugated polymer. *Adv. Mater.* **2018**, *30*, 1804556.
(13) Shi, C.; Soltani, S.; Armani, A. M. Gold nanorod plasmonic upconversion microlaser. *Nano Lett.* **2013**, *13*, 5827−5831.
(14) Yang, L.; Vahala, K. J. Gain functionalization of silica microresonators. *Opt. Lett.* **2003**, *28*, 592−594.
(15) Fernandez-Bravo, A.; Yao, K.; Barnard, E. S.; Borys, N. J.; Levy, E. S.; Tian, B.; Tajon, C. A.; Moretti, L.; Altoe, M. V.; Aloni, S.; Beketayev, K.; Scotognella, F.; Cohen, B. E.; Chan, E. M.; Schuck, P. J. Continuous-wave upconverting nanoparticle microlasers. *Nat. Nanotechnol.* **2018**, *13*, 572−577.
(16) Zhu, S.; Shi, L.; Xiao, B.; Zhang, X.; Fan, X. All-optical tunable microlaser based on an ultrahigh-Q erbium-doped hybrid microbottle cavity. *ACS Photonics* **2018**, *5*, 3794−3800.
(17) Kang, S.; Ouyang, T.; Yang, D.; Pan, Q.; Qiu, J.; Dong, G. Enhanced 2 μm mid-infrared laser output from Tm^{3+}-activated glass ceramic microcavities. *Laser Photonics Rev.* **2020**, *14*, 1900396.
(18) Chen, X.; Jin, L.; Kong, W.; Sun, T.; Zhang, W.; Liu, X.; Fan, J.; Yu, S. F.; Wang, F. Confining energy migration in upconversion nanoparticles towards deep ultraviolet lasing. *Nat. Commun.* **2016**, *7*, 10304.
(19) Shang, Y.; Zhou, J.; Cai, Y.; Wang, F.; Fernandez-Bravo, A.; Yang, C.; Jiang, L.; Jin, D. Low threshold lasing emissions from a single upconversion nanocrystal. *Nat. Commun.* **2020**, *11*, 6156.
(20) De Dood, M.; Slooff, L.; Polman, A.; Moroz, A.; Van Blaaderen, A. Local optical density of states in SiO_2 spherical microcavities: theory and experiment. *Phys. Rev. A: At., Mol., Opt. Phys.* **2001**, *64*, 033807.
(21) Gu, F.; Xie, F.; Lin, X.; Linghu, S.; Fang, W.; Zeng, H.; Tong, L.; Zhuang, S. Single whispering-gallery mode lasing in polymer bottle microresonators via spatial pump engineering. *Light: Sci. Appl.* **2017**, *6*, e17061.
(22) Choi, J. H.; Chang, S.; Kim, K. H.; Choi, W.; Lee, S. J.; Lee, J. M.; Hwang, M. S.; Kim, J.; Jeong, S.; Seo, M. K.; Choi, W.; Park, H. G. Selective pump focusing on individual laser modes in microcavities. *ACS Photonics* **2018**, *5*, 2791−2798.
(23) Lun, Y.; Zhan, Z.; Gu, F.; Wang, P.; Yu, H.; Li, Z. Cavity mode manipulated by single gold nanoparticles. *APL Photonics* **2020**, *5*, 061304.
(24) Gao, Z.; Zhang, W.; Yan, Y.; Yi, J.; Dong, H.; Wang, K.; Yao, J.; Zhao, Y. Proton-controlled organic microlaser switch. *ACS Nano* **2018**, *12*, 5734−5740.
(25) Zhang, Y.; Gong, X.; Yuan, Z.; Wang, W.; Chen, Y. DNA self-switchable microlaser. *ACS Nano* **2020**, *14*, 16122−16130.
(26) Carlon Zambon, N.; St-Jean, P.; Milićević, M.; Lemaître, A.; Harouri, A.; Le Gratiet, L.; Bleu, O.; Solnyshkov, D. D.; Malpuech, G.; Sagnes, I.; Ravets, S.; Amo, A.; Bloch, J. Optically controlling the emission chirality of microlasers. *Nat. Photonics* **2019**, *13*, 283−288.
(27) Hodaei, H.; Miri, M. A.; Heinrich, M.; Christodoulides, D. N.; Khajavikhan, M. Parity-time-symmetric microring lasers. *Science* **2014**, *346*, 975−978.
(28) Tang, B.; Dong, H.; Sun, L.; Zheng, W.; Wang, Q.; Sun, F.; Jiang, X.; Pan, A.; Zhang, L. Single-mode lasers based on cesium lead halide perovskite submicron spheres. *ACS Nano* **2017**, *11*, 10681−10688.
(29) Zhang, J.; Peng, B.; Özdemir, Ş. K.; Pichler, K.; Krimer, D. O.; Zhao, G.; Nori, F.; Liu, Y.; Rotter, S.; Yang, L. A phonon laser operating at an exceptional point. *Nat. Photonics* **2018**, *12*, 479−484.
(30) Yuan, Z.; Wang, H.; Wu, L.; Gao, M.; Vahala, K. J. Linewidth enhancement factor in a microcavity Brillouin laser. *Optica* **2020**, *7*, 1150−1153.

(31) Shen, X.; Choi, H.; Chen, D.; Zhao, W.; Armani, A. M. Raman laser from an optical resonator with a grafted single-molecule monolayer. *Nat. Photonics* **2020**, *14*, 95−101.
(32) Zhang, P.; Ji, Q.; Cao, Q.; Wang, H.; Liu, W.; Gong, Q.; Xiao, Y. Single-mode characteristic of a supermode microcavity Raman laser. *Proc. Natl. Acad. Sci. U. S. A.* **2021**, *118*, e2101605118.
(33) Asano, M.; Takeuchi, Y.; Chen, W.; Özdemir, Ş. K.; Ikuta, R.; Imoto, N.; Yang, L.; Yamamoto, T. Observation of optomechanical coupling in a microbottle resonator. *Laser Photonics Rev.* **2016**, *10*, 603−611.
(34) O'Shea, D.; Junge, C.; Volz, J.; Rauschenbeutel, A. Fiber-optical switch controlled by a single atom. *Phys. Rev. Lett.* **2013**, *111*, 193601.
(35) Yacomotti, A.; Furfaro, L.; Hachair, X.; Pedaci, F.; Giudici, M.; Tredicce, J.; Javaloyes, J.; Balle, S.; Viktorov, E. A.; Mandel, P. Dynamics of multimode semiconductor lasers. *Phys. Rev. A: At., Mol., Opt. Phys.* **2004**, *69*, 053816.
(36) Zhu, S.; Shi, L.; Yuan, S.; Xu, X.; Zhang, X. All-optical control of ultrahigh-Q silica microcavities with iron oxide nanoparticles. *Opt. Lett.* **2017**, *42*, 5133−5136.
(37) Kippenberg, T. J.; Kalkman, J.; Polman, A.; Vahala, K. J. Demonstration of an erbium-doped microdisk laser on a silicon chip. *Phys. Rev. A: At., Mol., Opt. Phys.* **2006**, *74*, 051802.
(38) Min, B.; Kippenberg, T. J.; Yang, L.; Vahala, K. J.; Kalkman, J.; Polman, A. Erbium-implanted high-Q silica toroidal microcavity laser on a silicon chip. *Phys. Rev. A: At., Mol., Opt. Phys.* **2004**, *70*, 033803.
(39) Sumetsky, M.; Dulashko, Y.; Windeler, R. S. Super free spectral range tunable optical microbubble resonator. *Opt. Lett.* **2010**, *35*, 1866−1868.
(40) Zhu, S.; Shi, L.; Ren, L.; Zhao, Y.; Jiang, B.; Xiao, B.; Zhang, X. Controllable Kerr and Raman-Kerr frequency combs in functionalized microsphere resonators. *Nanophotonics* **2019**, *8*, 2321−2329.
(41) Yang, Y.; Lei, F.; Kasumie, S.; Xu, L.; Ward, J. M.; Yang, L.; Nic Chormaic, S. Tunable erbium-doped microbubble laser fabricated by sol-gel coating. *Opt. Express* **2017**, *25*, 1308−1313.
(42) Liu, Y.; Yan, X.; Wu, J.; Zhu, B.; Chen, Y.; Chen, X. On-chip erbium-doped lithium niobate microcavity laser. *Sci. China: Phys., Mech. Astron.* **2021**, *64*, 234262.
(43) Yang, L.; Armani, D. K.; Vahala, K. J. Fiber-coupled erbium microlasers on a chip. *Appl. Phys. Lett.* **2003**, *83*, 825−826.
(44) Bekker, C. J.; Baker, C. G.; Bowen, W. P. Optically tunable photoluminescence and up-conversion lasing on a chip. *Phys. Rev. Appl.* **2021**, *15*, 034022.
(45) Lu, Q.; Wu, X.; Liu, L.; Xu, L. Mode-selective lasing in high-Q polymer micro bottle resonators. *Opt. Express* **2015**, *23*, 22740−22745.
(46) Wu, T.; Gurioli, M.; Lalanne, P. Nanoscale light confinement: the Q's and V's. *ACS Photonics* **2021**, *8*, 1522−1538.
(47) Rokhsari, H.; Vahala, K. J. Ultralow loss, high Q, four port resonant couplers for quantum optics and photonics. *Phys. Rev. Lett.* **2004**, *92*, 253905.
(48) Pöllinger, M.; Rauschenbeutel, A. All-optical signal processing at ultra-low powers in bottle microresonators using the Kerr effect. *Opt. Express* **2010**, *18*, 17764−17775.
(49) Zhang, X.; Cao, Q.; Wang, Z.; Liu, Y.; Qiu, C.; Yang, L.; Gong, Q.; Xiao, Y. Symmetry-breaking-induced nonlinear optics at a microcavity surface. *Nat. Photonics* **2019**, *13*, 21−24.
(50) Senthil Murugan, G.; Wilkinson, J. S.; Zervas, M. N. Selective excitation of whispering gallery modesin a novel bottle microresonator. *Opt. Express* **2009**, *17*, 11916−11925.
(51) Murugan, G. S.; Wilkinson, J. S.; Zervas, M. N. Optical excitation and probing of whispering gallery modes in bottle microresonators: potential for all-fiber add-drop filters. *Opt. Lett.* **2010**, *35*, 1893−1895.
(52) Lu, Q.; Chen, X.; Xie, S.; Wu, X. Controllable and selective single-mode lasing in polymer microbottle resonator. *Opt. Express* **2018**, *26*, 20183−20191.
(53) Xie, F.; Yao, N.; Fang, W.; Wang, H.; Gu, F.; Zhuang, S. Single-mode lasing via loss engineering in fiber-taper-coupled polymer bottle microresonators. *Photonics Res.* **2017**, *5*, 29−33.

https://doi.org/10.1021/acsphotonics.1c01096
ACS Photonics XXXX, XXX, XXX−XXX